JOURNAL OF SOLID STATE CHEMISTRY 89, 328–339 (1990)

# Structure, Electrical Transport, and Magnetic Properties of the Misfit Layer Compound $(CeS)_{1.16}NbS_2$, "$CeNbS_3$"

G. A. WIEGERS,* A. MEETSMA, R. J. HAANGE, AND J. L. DE BOER

*Laboratory of Inorganic Chemistry, Materials Science Center of the University, Nijenborgh 16, 9747 AG Groningen, The Netherlands*

Received April 9, 1990

$(CeS)_{1.16}NbS_2$ is a misfit layer compound built of alternate double layers of CeS, approximately a {100} slice of NaCl type CeS, and sandwiches of $NbS_2$ with Nb in slightly distorted trigonal prisms of sulfur. The two structural units in the composite crystal are described in centered orthorhombic lattices: $a_1$ = 5.727(1) Å, $b_1$ = 5.765(1) Å, $c_1$ = 11.41(1) Å, space group $Cm2a$, $Z$ = 4 for the CeS lattice and $a_2$ = 3.311(1) Å, $b_2$ = 5.765(1) Å, $c_2$ = 22.82(2) Å, space group $Fm2m$, $Z$ = 4 for the $NbS_2$ lattice. Corresponding axes are parallel and the stacking direction is $c$. Refinements of the CeS part, the $NbS_2$ part, and the common projection using 889, 288, and 135 reflections, respectively, converged to $R_F$ = 0.048, 0.069, and 0.072, respectively. The electrical conduction is metallic with a strong anisotropy, the resistivity along the $c$ axis, $\rho_c$, being about $10^4$ larger than the in-plane resistivity $\rho_{ab}$. The conduction is by holes in an almost filled $4d_{z^2}$ band of the $NbS_2$ part of the structure, indicating electron transfer from the CeS part to the $NbS_2$ part of the structure. The magnetic properties show down to 80 K a Curie Weiss behavior with a Curie constant close to that of CeS with the scheme $Ce^{3+}$ $(e^-)S^{2-}$; $\chi^{-1}$ goes to zero with decreasing temperature after a small discontinuous drop at about 50 K. 

## Introduction

Recent investigations (*1*) have shown that compounds formerly designated as ternary sulfides $MTS_3$ ($M$ = Sn, Pb, Bi rare earth metals; $T$ = Nb, Ta) are misfit layer compounds $(MS)_nTS_2$ ($n$ = 1.08–1.19) built of alternate double layers of $MS$ and sandwiches of $TS_2$ as occur in 2H-$NbS_2$ and 2H-$TaS_2$. The diffraction patterns of the compounds are described by two centered orthorhombic lattices; the unit cells have the $b$ axes in common while the $c$ axes (perpendicular to the crystal platelet) are equal or $c(TS_2)$ is twice $c(MS)$. The ratio of the length of the $a$ axes (the axes being parallel) is irrational but close to $\sqrt{3}$. So far three types were found which differ in the stacking of units along $c$; the structure types are designated by the centering types $C$ and $F$ of the two orthorhombic sublattices. The type indicated by $CC$ with both the $MS$ and the $TS_2$ lattice $C$-centered orthorhombic is found for $(SnS)_{1.17}NbS_2$ (*2*); the $CF$ type with a $C$-centered $MS$ lattice and an $F$-centered $TS_2$ lattice, $c(TS_2)$ being twice $c(MS)$, is found for $(LaS)_{1.14}NbS_2$ and $(PbS)_{1.14}NbS_2$ (*3*) and $(LaS)_{1.13}TaS_2$ and $(CeS)_{1.15}TaS_2$ (*4*), (unit cell dimensions are given in Table I) while the $FF$-type with both lattices $F$ centered is found for $(PbS)_{1.13}TaS_2$ (*5*) and $(SmS)_{1.19}TaS_2$ (*6*). The composition of the

* To whom correspondence should be addressed.

0022-4596/90 $3.00

TABLE I

CRYSTAL DATA OF $(LaS)_{1.14}NbS_2$, $(LaS)_{1.13}TaS_2$, $(CeS)_{1.16}NbS_2$, AND $(CeS)_{1.15}TaS_2$. STANDARD DEVIATIONS ARE IN PARENTHESES

| Compound | Lattice | a(Å) | b(Å) | c(Å) | Space group | Z |
|---|---|---|---|---|---|---|
| $(LaS)_{1.14}NbS_2$ | LaS | 5.828(1) | 5.799(1) | 11.512(2) | *Cm2a* | 4 |
| | $NbS_2$ | 3.310(1) | 5.793(2) | 23.043(9) | *Fm2m* | 4 |
| $(LaS)_{1.13}TaS_2$ | LaS | 5.831(1) | 5.773(1) | 11.526(1) | *Cm2a* | 4 |
| | $TaS_2$ | 3.295(1) | 5.778(1) | 23.057(1) | *Fm2m* | 4 |
| $(CeS)_{1.16}NbS_2$ | CeS | 5.727(1) | 5.765(1) | 11.41(1) | *Cm2a* | 4 |
| | $NbS_2$ | 3.311(1) | 5.765(1) | 22.82(2) | *Fm2m* | 4 |
| $(CeS)_{1.15}TaS_2$ | CeS | 5.737(1) | 5.749(1) | 11.444(2) | *Cm2a* | 4 |
| | $TaS_2$ | 3.329(1) | 5.749(1) | 22.892(2) | *Fm2m* | 4 |

compounds is determined by the ratio of the length of the *a* axes (the misfit axes) and the number of formula units per cell.

$(CeS)_{1.16}NbS_2$ described in this paper was prepared first by Meerschaut, Rabu, and Rouxel (*7*); these authors found an orthorhombic unit cell with space group *Bbcb* and lattice parameters: $a = 23.127$ Å, $b = 5.775$ Å, and $c = 22.877$ Å. The powder diffraction pattern showed that reflections *hkl* occur for $h = 0$; $h = 4$, mod 4; and $h = 7$, mod 7, which already suggests that the structure consists of two separate parts. In the same paper the structure determination of $(LaS)_{1.14}NbS_2$ using single crystal X-ray diffraction was reported; the unit cell dimensions: $a = 23.216$ Å, $b = 5.806$ Å, $c = 23.031$ Å are close to those found for $(CeS)_{1.16}NbS_2$. The agreement between the observed and calculated structure factors of $(LaS)_{1.14}NbS_2$ was good for reflections $h = 4$, mod 4 but rather bad for the $h = 0$ and $h = 7$, mod 7 reflections. A reinvestigation (*3*) of the diffraction data of $(LaS)_{1.14}NbS_2$ was performed in terms of a composite crystal with a LaS part with an orthorhombic cell with $a_1 = a/4$, $b_1 = b$, $c_1 = c/2$, and space group *Cm2a* and a $NbS_2$ part with $a_2 = a/7$, $b_2 = b$, $c_2 = c$ and space group *Fm2m*. Refinements converged to $R_F = 0.048$ and 0.087, respectively, for reflections of the LaS and $NbS_2$ part, respectively, and to 0.067 for the 0*kl* reflections which are common to both parts. Single crystal refinements of $(LaS)_{1.13}TaS_2$ and $(CeS)_{1.15}TaS_2$ showed these compounds also to belong to the *CF* type misfit layer compounds (*4*). The symmetry of the complete structure, including the mutual modulation of the two sublattices was analyzed in terms of a four-dimensional space group.

In this paper the structure determination by single crystal X-ray diffraction, the electrical transport, and the magnetic properties of $(CeS)_{1.16}NbS_2$ are described.

## Experimental

$(CeS)_{1.16}NbS_2$ was prepared from the elements at about 1100°C. Crystals suitable for single crystal X-ray diffraction and electrical transport measurements were grown by vapor transport using $Cl_2$ as transport agent. $(NH_4)_2PbCl_6$ was used as a source of chlorine; to about 300 mg of the starting material about 10 mg $(NH_4)_2PbCl_6$ was added. Crystals grow as thin platelets at the low temperature side of a gradient of 1100 to 900°C. Physical properties were measured with apparatus described extensively in our paper on structure and properties of $(PbS)_{1.13}TaS_2$ (*5*); SI units are used throughout.

## The Structure Determination of $(CeS)_{1.16}NbS_2$

Single crystal X-ray diffraction with an Enraf–Nonius CAD-4F diffractometer using monochromatized Mo$K\bar{\alpha}$ ($\lambda = 0.71073$ Å) radiation of a crystal of approximate dimensions of $0.20 \times 0.27 \times 0.006$ mm$^3$ revealed that the reflections can be indexed using two orthorhombic unit cells with the axes parallel and cell constants as given in Table I. The *c* axes are perpendicular to the crystal platelet. In the *a*–*b* plane the two lattices have the *b* axis in common, while the ratio of the lengths of the *a* axes ($a_1/a_2$) being 5.727/3.311 = 1.7296 (s.d. 0.0006) is

irrational. Along the direction of the $c$ axes the length $c_2 = 2c_1$. Because the ratio of the length of the $a$ axes deviates significantly from the ratio 7/4 (= 1.75) it is not justified to choose a supercell with $a \approx 4a_1 \approx 7a_2$ as proposed by Meerschaut *et al.* (*7*). The structure determination proceeds in three different parts, viz., the structure determination of the CeS and $NbS_2$ part separately, during which the common $0kl$ reflections were omitted because their intensities are determined by both lattices together, followed by a determination of the relative origin of both structure parts in the complete structure, using the common $0kl$ reflections. This procedure has been described in our paper on $(SnS)_{1.17}NbS_2$ with the *CC* type structure (*2*).

*The CeS Part*

Unit cell dimensions and their standard deviations were determined from the setting angles of 12 reflections in the range $22.91° < \theta < 25.80°$ in four alternate settings (*8*). All reflections were measured in one hemisphere up to $\theta = 50°$. There was no indication of crystal decomposition and the intensity of the reference reflections showed only a small fluctuation about the mean value during the 100.6 hr of X-ray exposure time. A 360° $\psi$-scan for the reflection (400) close to axial showed an intensity variation up to 17% about the mean value. The net intensities of the data were corrected for the scale variation, Lorentz and polarization effects, and for absorption using a Gaussian integration method (grid: 8 × 8 × 4) (*9*). Standard deviations in the intensities based on counting statistics were increased according to an analysis of the excess variance of the two reference reflections: $\sigma^2(I) = \sigma^2_{cs}(I) + (PI)^2$, where $P$ (= 0.0083) is the instability constant (*10*). Averaging equivalent reflections resulted in 1117 unique reflections. In space group *Cm2a* (No. 39 of the *International Tables for X-Ray Crystallography*, 1983 (*11*), the atoms are on site 4*c*: *1/4,y,z*. As a choice of the origin $y$ of Ce was chosen equal to zero. Refinements on $F$ by full-matrix least-squares with 889 unique reflections with $I \geq 2.5\ \sigma(I)$ converged at $R_F = 0.048$, $wR = 0.050$, $S = 2.133$; the weighting scheme was $w = 1$. Reflections with $((||F_o|| - ||F_c||) > 15)$ were excluded from the final refinement cycle. Cell data and details of data collection and refinement are given in Tables I–III. Final fractional coordinates are given in Table V.

*The $NbS_2$ Part*

Unit cell dimensions and their standard deviations were determined from the setting angles of 23 reflections in the range $25.39° < \theta < 27.73°$ in four alternate settings (*8*). All reflections were measured in one hemisphere up to $\theta = 40°$. The two reference reflections measured every 2 hr showed a long term variation of less then 1% during the 26.3 hr of X-ray exposure time. Corrections were applied as described for the CeS part. In space group *Fm2m* (No. 42 of (*11*) Nb is 4*a*: 0,$y'$,0 and S is at 4*c*: 0,$y'$,$z'$. One of the $y'$ coordinates may be chosen arbitrarily; at this stage $y' = 0$ was chosen for Nb. Refinements by full-matrix least-squares using 282 unique reflections converged at $R_F = 0.069$, $wR = 0.088$, $S = 5.216$; unit weights were applied. Reflections with $(||F_o|| - ||F_c|| > 15)$ were excluded from the final refinement cycle. Cell data and data collection and refinement details are given in Tables I–III. Final fractional coordinates and temperature factors are given in Table V; the $y'$ coordinates are given with respect to those of CeS with Ce at $y = 0$ (see next section).

*The Complete Structure*

From the size of the unit cells in the $a$–$b$-plane and the number of formula units CeS and $NbS_2$ per cell one finds that the composition of the compound is $(CeS)_{1.16}NbS_2$ (viz.,

TABLE II

DATA COLLECTION OF $(CeS)_{1.16}NbS_2$

| | CeS part | | $NbS_2$ part |
|---|---|---|---|
| Diffractometer | | Enraf-Nonius CAD-4F | |
| Radiation (Å) | | Mo$K\bar{\alpha}$, *0.71073* | |
| Monochromator | | Graphite | |
| Temperature (K) | | 295 | |
| Range; minimum maximum (deg) | 1.7, 50.0 | | 1.79, 40 |
| $\omega/2\theta$ scan (deg) | | $\Delta\omega = 1.10 + 0.35 \text{ tg } \theta$ | |
| Data set | $h$: $0 \rightarrow 12$; $k$: $-12 \rightarrow 12$; $l$: $-24 \rightarrow 24$ | | $h$: $0 \rightarrow 5$; $k$: $-10 \rightarrow 10$ $l$: $-40 \rightarrow 40$ |
| Crystal to receiving | | | |
| Aperture distance (mm) | | 173 | |
| Horizontal, vertical aperture (mm) | | 4.2, 4.5 | |
| Reference reflections (rms dev. in %) | 0.24; 0.95 | | 024, 1.53 |
| | 0.24; 0.47 | | 024, 0.82 |
| Instability constant, $P$ | 0.0083 | | 0.0167 |
| Drift correction | 0.997–1.000 | | 1.000–1.063 |
| Minimum and maximum absorption correction factor | | 1.10–4.35 | |
| X-ray exposure time (hr) | 100.6 | | 26.3 |
| Total data | 4191 | | 1499 |
| Unique data | 1117 | | 410 |

1.16 = 2 * (3.311/5.752)). Since the 0$kl$ reflections are only present for $k = 2n$, a smaller unit cell can be chosen for the refinement, viz. the unit cell with $b'' = (1/2)b_1$, $c'' = c_1 = (1/2)\ c_2$); this unit cell contains one unit $NbS_2$ and 1.16 units CeS. The two-dimensional space group is $Pm$ (No. 3 of the 17 two-dimensional space groups (*11*). For the refinement using XTAL a three-dimensional space group had to be chosen; the space group in agreement with the projection is $P11m$ (*11*) with the midplane of the double layer of CeS at the mirror plane at $z'' = 1/2$ and niobium of the $NbS_2$ sandwich at $z'' = 0$. In this way Nb is at site 1$a$ while other atoms are at 2$c$. The $y''$ coordinate of Ce was fixed at $y'' = 0$ and S(1) of the CeS unit at $y'' = -0.006$ (the difference in $y''$

TABLE III

DETAILS OF THE REFINEMENT OF THE CeS AND $NbS_2$ PARTS

| | CeS | $NbS_2$ |
|---|---|---|
| Number of reflections: $h \neq 0$ | 889 | 288 |
| Number of refined parameters | 12 | 10 |
| Final agreement factors: | | |
| $R_F = \Sigma(\|\|F_0\| - \|F_c\|\|)/\Sigma\|F_0\|$ | 0.048 | 0.069 |
| $wR = [\Sigma(w(\|F_0\| - \|F_c\|)^2)/\Sigma w\|F_0\|^2]^{1/2}$ | 0.050 | 0.069 |
| Weighting scheme | 1 | 1 |
| $S = [\Sigma w(\|F_0\| - \|F_c\|)^2/(m - n)]^{1/2}$ | 2.133 | 5.216 |
| $m$ = number of observations | | |
| $n$ = number of variables | | |
| Minimum and maximum residual densities in final difference Fourier map, $e/Å^3$ | −3.2, 3.2 | −8.23, 9.45 |
| Maximum (shift/sigma) final cycle | $0.27 \times 10^{-4}$ | $0.53 \times 10^{-3}$ |
| Average (shift/sigma) final cycle | $0.12 \times 10^{-4}$ | $0.96 \times 10^{-4}$ |

following from the CeS refinement taking into account the ratio of two in the length of the $b$ axes). The starting values of the $z''$ coordinates of Ce(1) and S(1) followed from the CeS refinement. Starting values for the $y''$ coordinates of Nb(1) and S(2) of the $NbS_2$ lattice are from isostructural $(LaS)_{1.14}NbS_2$ (*3*); the $z''$ coordinate of S(2), $z'' = 0.1374$, is from the $NbS_2$ refinement. Parameters in the full-matrix least-squares refinement were the coordinates, except $y''$ of Ce(1) and S(1) and $z''$ of Nb(1), the site occupancy factor (s.o.f.) of Ce(1) and S(1) (kept equal), and the isotropic thermal parameters of all atoms. The refinement converged to $R_F = 0.70$, $wR = 0.078$ for 135 $0kl$ reflections. The $z$ coordinates are within the standard deviation equal to those of the CeS and $NbS_2$ refinements taking into account the different unit cells. The composition of the compound obtained from the occupancy of the Ce(1) and S(1) sites (0.51 s.d. 0.01) is not in good agreement with the occupancy, 0.58, calculated from the ratio of the lengths of the $a$-axes of the two structural units. It is also visible in the ratio of the scale factors for the CeS and $NbS_2$ refinements (see the supplementary material). The same phenomenon was observed for similar structure determinations of misfit layer compounds (*3–6*). A possible explanation is stacking disorder which must be mainly in the CeS lattice, in order to explain the observed s.o.f. Another possibility is the effect of the mutual modulation which is in the average structure visible in the anisotropic temperature factors of the atoms, viz., $U_{11}$ is always larger than $U_{22}$ and $U_{33}$, which is understandable considering that the modulation is along the $a$ axes. It is also seen that $U_{11}$ of Ce(1) and S(1) is larger than $U_{11}$ of Nb(1) and S(2), which indicates that the CeS lattice is strongest modulated. A stronger modulation of the CeS lattice leads to a stronger decrease of the intensities of the CeS reflections, which is visible in the ratio of the scale factors for CeS and $NbS_2$. In the structure factor of the $0kl$ reflections, Ce(1) and S(1) will have a smaller contribution than expected from the ratio of the length of the misfit axes, as indeed observed. Crystal data and experimental details of this part of the structure determination are compiled in Table IV. Final fractional atomic coordinates and equivalent isotropic thermal parameters and s.o.f.'s are given in Table V. It is now possible to change the $y'$ coordinates of the $NbS_2$ lattice with respect to those of CeS with Ce at $y = 0$. This is done by halving the $y''$ coordinate of Nb: $y' = (1/2)\,y''$; the $y'$ coordinate of S(2) is changed accordingly. It may be noted that in this way the structure is completely described by the tables for the CeS and $NbS_2$ parts.[1]

TABLE IV

DETAILS OF THE REFINEMENT OF THE PROJECTION ALONG [100] ($b$ = 2.883(1) Å, $c$ = 11.41(1) Å, SPACE GROUP $P11m$, $Z$ = 1)

| | |
|---|---|
| Number of reflections, $h = 0$ | 135 |
| Number of refined parameters | 7 |
| Final agreement factors: | |
| $R_F = \Sigma(\|\|F_0\| - \|F_c\|\|)/\Sigma\|F_0\|$ | 0.072 |
| $wR = [\Sigma(w(\|F_0\| - \|F_c\|)^2)/\Sigma w\|F_0\|^2]^{1/2}$ | 0.078 |
| Weighting scheme | 1 |
| $S = [\Sigma w(\|F_0\| - \|F_c\|)^2/(m - n)]^{1/2}$ | 1.827 |
| $m$ = number of observations | |
| $n$ = number of variables | |
| Residual electron density in final difference Fourier map, $e/Å^3$ | −1.14, 1.29 |
| Maximum (shift/sigma) final cycle | $0.78 \times 10^{-2}$ |
| Average (shift/sigma) final cycle | $0.15 \times 10^{-2}$ |

In all our calculations scattering factors were taken from Cromer and Mann (*12*). Anomalous dispersion factors are those given by Cromer and Liberman (*13*). All cal-

[1] See NAPS document No. 04813 for 13 pages of supplementary material ($F_0$, $F_c$). Order from ASIS/NAPS Microfiche Publications, P.O. Box 3513, Grand Central Station, New York, NY 10163. Remit in advance $4.00 for microfiche or photocopy, $7.75 up to 20 pages plus $.30 for each additional page. All orders must be prepaid.

TABLE V

ATOMIC POSITIONS AND TEMPERATURE FACTORS OF $(CeS)_{1.16}NbS_2$

$U_{eq} = 1/3\Sigma_i\Sigma_j U_{ij}a^*_i a^*_j \mathbf{a}_i \cdot \mathbf{a}_j$.
Thermal vibration amplitudes (Å$^2$)
$F(h) = F_0(h) \exp(-8\pi^2 U_{iso} (\sin(\theta)/\lambda)^2)$ or
$F(h) = F_0(h) \exp(-2\pi^2 \sum_{i=1}^{3}\sum_{j=1}^{3} h_i h_j a^*_i a^*_j U_{ij})$

CeS

| | $x$ | $y$ | $z$ |
|---|---|---|---|
| Ce(1) | 1/4 | 0.0 (−) | 0.65205(3) |
| S(1) | 1/4 | −0.503(1) | 0.5999(1) |

| | $U_{11}$ | $U_{22}$ | $U_{33}$ | $U_{23}$ |
|---|---|---|---|---|
| Ce(1) | 0.0210(2) | 0.0160(2) | 0.0084(1) | 0.0016(5) |
| S(1) | 0.0171(6) | 0.0108(8) | 0.0079(5) | 0.004(1) |

$NbS_2$

| | $x'$ | $y'$ | $z'$ |
|---|---|---|---|
| Nb(1) | 0 | −0.07585(−) | 0 |
| S(1) | 0 | 0.2561(7) | 0.0687(1) |

| | $U_{11}$ | $U_{22}$ | $U_{33}$ | $U_{23}$ |
|---|---|---|---|---|
| Nb(1) | 0.0141(6) | 0.0014(6) | 0.0005(5) | 0.00000(0) |
| S(1) | 0.016(1) | 0.004(1) | 0.002(1) | 0.001(1) |

Common part
(Coordinates in a unit cell with $b''$ = 2.883(1) Å, $c''$ = 11.41(1) Å)

| | $x''$ | $y''$ | $z''$ | s.o.f. | $U_{iso}$(Å$^2$) |
|---|---|---|---|---|---|
| Ce(1) | — | 0.0(−) | 0.6520(2) | 0.515(11) | 0.0123(7) |
| S(1) | — | −0.006(−) | 0.401(1) | 0.515(11) | 0.007(2) |
| Nb(1) | — | −0.1517(15) | 0 | 1.0 | 0.0045(5) |
| S(2) | — | −0.485(3) | 0.1369(5) | 1.0 | 0.007(1) |

*Note.* Values of the fractional coordinates of the CeS and $NbS_2$ parts are with respect to the unit cell defined in Table I. The e.s.d.s are given in parentheses; for coordinates fixed by choice by (−), coordinates fixed by symmetry have no s.d.

culations are carried out on the CDC-Cyber 170/760 computer of the University of Groningen with the program packages XTAL (*14*) and EUCLID (*15*) for the calculation of geometric data.

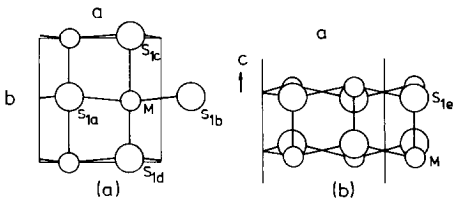


FIG. 1. The CeS double layer of $(CeS)_{1.16}NbS_2$ projected (a) along [001], only the upper half of the double layer is shown for the sake of clarity and (b) along [100]; large open circles are S atoms.

## Discussion of the Structure

$(CeS)_{1.16}NbS_2$ belongs to the *CF* structure type of misfit layer compounds with centered orthorhombic lattices; the compound is isostructural with $(LaS)_{1.14}NbS_2$ and $(PbS)_{1.14}NbS_2$ (*3*), disregarding the disorder in the $NbS_2$ lattice of the latter compound, and with $(LaS)_{1.13}TaS_2$ and $(CeS)_{1.15}TaS_2$ (*4*). It is built of alternate double layers of CeS (Fig. 1) and sandwiches of $NbS_2$ with Nb in trigonal prisms of S as Nb in 2H-$NbS_2$ (Fig. 2). The complete structure is shown in pro-

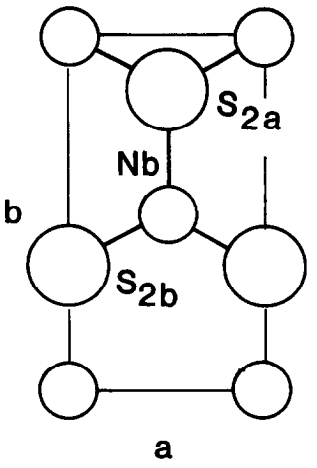


FIG. 2. A sandwich of $NbS_2$ in $(CeS)_{1.16}NbS_2$ with Nb at $y$ = 0 projected along [001]; large open circles are S atoms.

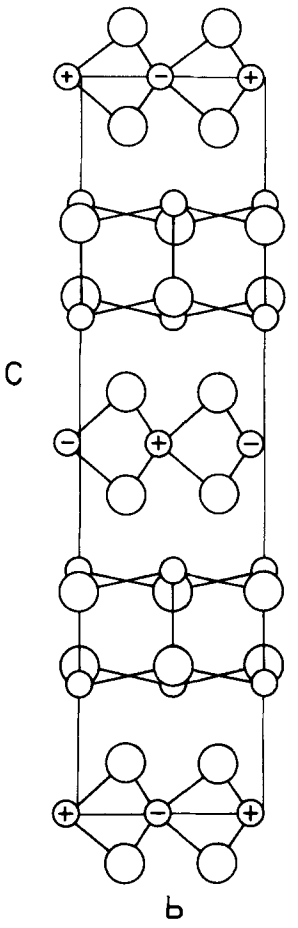


FIG. 3. Structure of $(CeS)_{1.16}NbS_2$ projected along the misfit [100] axes. In order to demonstrate the $F$ centering of the $NbS_2$ lattice, Nb atoms at $z = 0$ and $z = 1/2$ in the same plane parallel (100) have the same symbol (+ or −), whereas Nb atoms $(1/2)a_2$ apart have different symbols. Large open circles are S atoms.

jection along the misfit $a$ axes in Fig. 3. From this figure it is seen that Ce is coordinated by five sulfur atoms from the CeS double layer on the corners of a square pyramid; the Ce–S distances (Table VI) are close to those found in NaCl type CeS (values for the lattice constant of CeS range from 5.763 to 5.778 Å (*16*)). NaCl type CeS may be considered to be the parent substance of the CeS part since the double layer is a distorted

TABLE VI

DISTANCES[a] (IN Å) IN $(CeS)_{1.16}NbS_2$

| | | | | |
|---|---|---|---|---|
| $Ce–S_{1a}$ | 2.925(3) | $Nb–S_{2a}$ | 2.474(4) | (2x) |
| $Ce–S_{1b}$ | 2.925(3) | $Nb–S_{2b}$ | 2.477(3) | (4x) |
| $Ce–S_{1c}$ | 2.96(1) | | | |
| $Ce–S_{1d}$ | 2.92(1) | | | |
| $Ce–S_{1e}$ | 2.875(3) | | | |

[a] The numbering of atoms refers to Figs. 1 and 2.

slab with a thickness of half the cell edge of *f.c.c.* CeS; the distortion is such that Ce atoms are protruding from the planes of sulfur atoms. The Ce atoms (at $y = 0$ and 1/2) are lying in groves parallel to $a$ formed by rows (at $y' = 0.256$ and 0.756) of sulfur atoms of neighboring $NbS_2$ sandwiches (Fig. 4). In this way each Ce atom is, in addition to the S atoms of the CeS double layer, also coordinated to sulfur atoms of neighboring $NbS_2$ sandwiches. Due to the incommensurate character of the structure along the $a$ axes, the number of coordinating sulfur atoms is two or three (Fig. 4). The total number of coordinating S atoms of each Ce is therefore seven or eight. The Nb–S distances in the sandwiches of $NbS_2$ (Table VI) are close (within about 0.01 Å) to those observed in $(SnS)_{1.17}NbS_2$ (*2*), $(LaS)_{1.14}NbS_2$ and $(PbS)_{1.14}NbS_2$ (*3*), and the intercalate $Ag_{0.6}NbS_2$ (*17*).

As discussed in our paper on $(PbS)_{1.14}NbS_2$ and $(LaS)_{1.14}NbS_2$ (*3*), and in a previous section, one expects besides the reflections of the two sublattices, also satellites due to their mutual modulation. Electron diffraction with the electron beam along the $c$ axes of the crystals clearly showed the presence of satellites at the expected positions (*1*). The satellites are weak, indicating that the modulation (of displacive nature) is small. The temperature factors of the various refinements indicate that the CeS lattice is the strongest modulated.

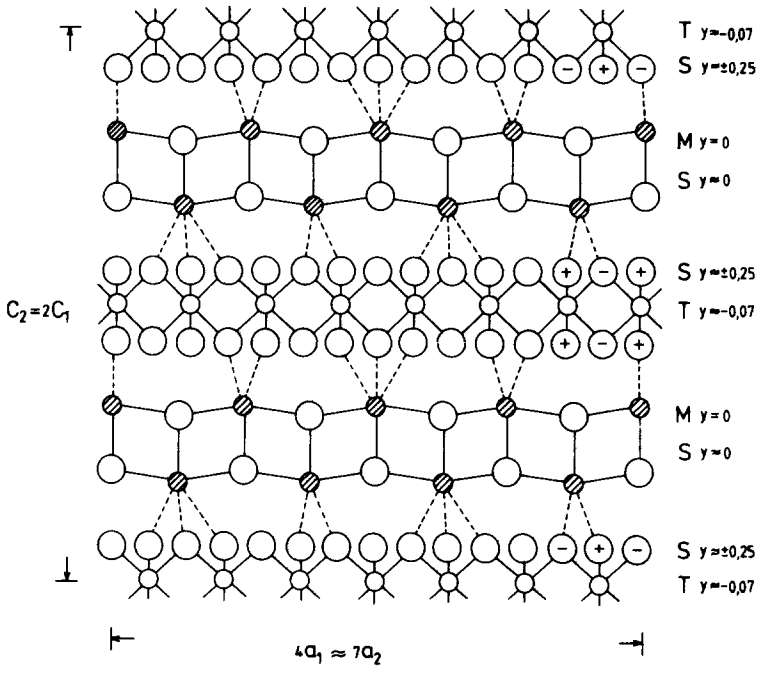


FIG. 4. Projection of part of the $(CeS)_{1.16}NbS_2$ structure along [010], showing the coordination of Ce by S of the CeS double layer and S of $NbS_2$. For the sake of clarity only the sheet of CeS parallel [100] at $y = 0$ for Ce and $y \approx 0$ for S(1) and the coordination of S(2) at $y \approx \pm 0.25$ by Nb at $y = -0.07$ is shown. Large open circles are S atoms. Ce and Nb atoms are indicated by small dashed and open circles, respectively.

## Electrical Transport Properties and Magnetic Properties

The electrical resistivity in the $a$–$b$-plane ($\rho_{ab}$) and the Hall coefficient $R_H$ were measured on two crystal platelets with a thickness of 14 and 18 $\mu$m using a four and five contact method for $\rho_{ab}$ and $R_H$ respectively. For Hall measurements the magnetic field was along the $c$ axis. The in-plane resistivity shows metallic behavior (Fig. 5). The relative low value of the resistivity ratio $\rho$(400 K)/$\rho$(4 K) of 2.4 and the large residual resistivity may indicate the presence of defects and/or atomic disorder. Measurements of the resistivity of other misfit layer compounds have shown that for some compounds the resistivity ratio $\rho$(300 K)/$\rho$(4 K) is as large as 12 while the residual resistivity is small, which indicates that a low resistivity ratio and high residual resistivity is not

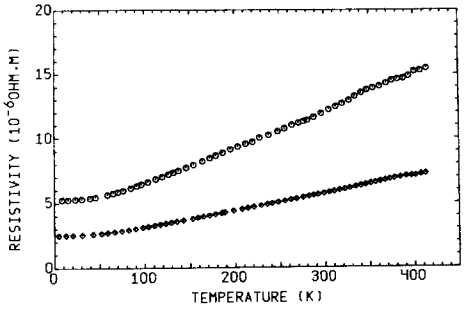


FIG. 5. The in-plane resistivity $\rho_{ab}$ of two crystals $(CeS)_{1.16}NbS_2$ versus temperature; circles and squares are for samples with thicknesses of 14 and 18 $\mu$m, respectively.

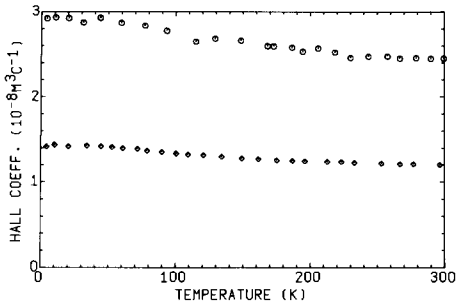


FIG. 6. The Hall coefficient $R_H$ versus temperature curve for two crystals $(CeS)_{1.16}NbS_2$. Circles and squares are for samples with thickness of 14 and 18 $\mu$m, respectively.

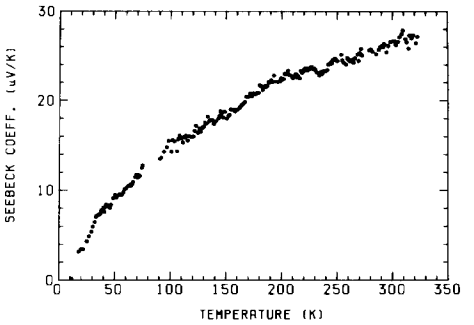


FIG. 8. The Seebeck coefficient of $(CeS)_{1.16}NbS_2$ versus temperature.

an intrinsic property of these compounds having no three-dimensional periodicity. $R_H$ versus temperature curves of the single crystal measurements are shown in Fig. 6. The values of $\rho_{ab}$ as well as $R_H$ for the two crystals differ by a factor of 2.3, probably due to the error in the measurement of the dimensions of the distances between contacts and in particular the thickness of the very thin crystals. The resistivity along the $c$ axis, $\rho_c$, measured using contacts on the two sides of a crystal (Fig. 7) is also metallic. The ratio $\rho_{ab}/\rho_c$ is about $10^4$. The resistivity and Hall coefficient were also measured on a powder compact of dimensions 4.4 × 2.4 × 0.26 $mm^3$ with strong preferred orientation of the powder particles ($ab$ planes parallel to the surface of dimensions 4.4 × 2.4 $mm^2$). For Hall measurements the magnetic field was therefore for the majority of the particles along the $c$ axis. The resistivity of the compact (not shown) is 10–30 times larger than $\rho_{ab}$ from single crystal measurements probably because of the deviation from a complete parallel orientation of the powder particles. The Hall coefficient of the compact is $10^{-8}$ $m^3C^{-1}$ at 300 K and 1.1 × $10^{-8}$ $m^3C^{-1}$ at 4 K (curve not shown). The Hall coefficient is in all cases positive and increases only slightly with decreasing temperature; the average of the two single crystal measurements is 1.8 × $10^{-8}$ $m^3C^{-1}$ at 300 K, and 2.1 × $10^{-8}$ $m^3C^{-1}$ at 4 K. The Seebeck coefficient ($\alpha$) measured on a powder compact is positive in the temperature range 4–300 K and amounts to about 30 $\mu VK^{-1}$ at 300 K (Fig. 8). The positive sign of $R_H$ and $\alpha$ indicates that the conduction is by holes. It is therefore justified to calculate the number of charge carries per unit volume using $R_H = 1/(ep)$, $p$ being the number of charge carriers per unit volume and $e$ the elemental charge. For $R_H = 1.0 \times 10^{-8}$ $m^3C^{-1}$ at 300 K (the powder compact), $p$ amounts to $6.25 \times 10^{26}$ $m^{-3}$, which corresponds with 0.07 hole per Nb atom. From the average $R_H$ of the single crystal measurements one calculates 0.04 h/Nb at 300 K. The hole number is calculated per Nb because the conduction is explained well by

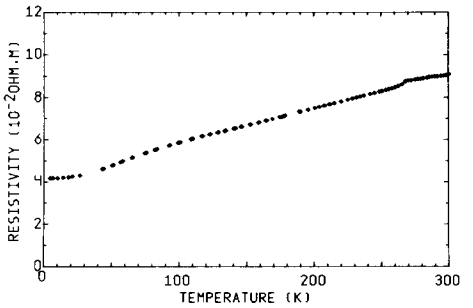


FIG. 7. The resistivity along the $c$ axis, $\rho_c$, of $(CeS)_{1.16}NbS_2$ versus temperature.

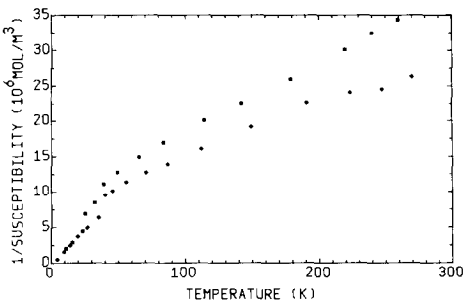


FIG. 9. The reciprocal magnetic susceptibility $\chi_{ab}^{-1}$ (■) and $\chi_c^{-1}$ (◆) versus temperature of $(CeS)_{1.16}NbS_2$ at a field of 0.875 T.

only taking into account the $NbS_2$ part of the structure, as will be discussed below. The mobility of the holes calculated from average $R_H$ and average $\rho_{ab}$ of the two single crystal measurements amounts to $2.0 \times 10^{-3}$ $m^2V^{-1}sec^{-1}$ at 300 K and $4.6 \times 10^{-3}$ $m^2V^{-1}sec^{-1}$ at 4 K.

The magnetic suscpetibility was measured on a powder compact which showed a strong preferred orientation of the powder particles. The susceptibility was therefore measured using the compact in two orientations with respect to the magnetic field (0.875 T) (Fig. 9). It is supposed that the measurements give good estimates of $\chi_c$ ($H$ parallel to $c$) and $\chi_{ab}$ ($H$ parallel to the $a$–$b$ plane). $M$ versus field measurements at 4.2, 7, and 10 K were linear, $M \sim H$, in the range up to 1 T. The reciprocal magnetic susceptibility $\chi_{ab}^{-1}$ versus temperature curve shows Curie–Weiss behavior in the range 50–300 K; the Curie constant is $12.0 \times 10^{-6}m^3Kmol^{-1}$ and the asymptotic Curie temperature is −85 K. The $\chi_c^{-1}$ versus temperature curve shows a deviation from a linear behavior for T > 200 K; the Curie constant is in the linear part of the curve $15.6 \times 10^{-6}$ $m^3Kmol^{-1}$. The small drop in $\chi^{-1}$ followed by a continuous decrease of $\chi^{-1}$ to zero was also observed for $(LaS)_{1.14}NbS_2$ (*18*), $(SmS)_{1.19}TaS_2$ (*6*), and $(GdS)_{1.21}NbS_2$ (*19*).

2H-$NbS_2$, the parent substance of $(CeS)_{1.16}NbS_2$, is a $p$ type metal. Band structure calculations (review given by Doni and Girlanda (*20*)) have shown that due to the trigonal-prismatic coordination of Nb by S the $d$ band of Nb is split up into a half-filled $4d_{z^2}$ band and an upper lying empty $d$ band. The $4d_{z^2}$ band overlaps the valence band made of mainly $3s$ and $3p$ of sulfur. The Hall coefficient of 2H-$NbS_2$ is positive and the Hall number, 1 h/Nb, is in agreement with a half-filled $4d_{z^2}$ band. The in-plane resistivity amounts to $1.1 \times 10^{-6}$ Ωm at 300 K (*21*). The magnetic properties are those of a high-density-of-states Pauli paramagnetic metal (*22*). 2H-$NbS_2$ does not show a charge density wave transition like 2H-$TaS_2$ at 80 K. 2H-$NbS_2$ becomes superconducting at 6 K (*23*).

CeS with rocksalt structure carries a single $4f$ electron (*16*). The second excess valence electron, delocalized in a partly filled $5d$ band is responsible for the metallic properties and influences the magnetic properties by modifying the exchange interactions. The magnetic properties of single crystals of CeS studied by Hulliger *et al.* (*16*) confirmed largely the powder measurements of Loginov *et al.* (*24*). The magnetic susceptibility shows Curie–Weiss behaviour with a Curie constant of $9.30 \times 10^{-6}$ $m^3Kmol^{-1}$, an asymptotic Curie temperature of −20 K and antiferromagnetic ordering at about 8 K (*16*). The Curie constant is reduced compared with the expected value $C = 10.1 \times 10^{-6}$ $m^3Kmol^{-1}$ for free $Ce^{3+}$ ions (*25*).

The electrical transport properties of $(CeS)_{1.16}NbS_2$ may be interpreted as being due to an almost (0.07–0.04 hole per Nb) filled $4d_{z^2}$ band of the $NbS_2$ part of the structure which corresponds to a donation of 0.93–0.96 electrons from the CeS part of the structure. Assuming Ce in the CeS part to be in the 3+ state, the number of electrons per Ce in the partly filled $5d$ conduction band is {1.16 − (0.96 to 0.93)} = 0.20 to 0.23. A second possibility is that Ce is present as

$Ce^{3+}$ ($4f^1$) and $Ce^{2+}$ ($4f^2$) in the ratio of about 4 to 1. Since the transport properties are well described by holes only, viz., those in the $4d_{z^2}$ band of $NbS_2$, these properties are in favor of 80% $Ce^{3+}$ and 20% $Ce^{2+}$ in the CeS double layer.

The Curie constants $C_{ab}$ and $C_c$ of $12.0 \times 10^{-6}$ $m^3Kmol^{-1}$ and $15.6 \times 10^{-6}$ $m^3Kmol^{-1}$ corresponding to values per mole of Ce of $10.4\ 10^{-6}$ $m^3Kmol^{-1}$ (Ce) and $13.4 \times 10^{-6}$ $m^3Kmol^{-1}$ (Ce), respectively, may be compared with the free $Ce^{3+}$ ion Curie constant of $10.1 \times 10^{-6}$ $m^3Kmol^{-1}$ (*25*) and the Curie constant $9.3 \times 10^{-6}$ $m^3Kmol^{-1}$ of CeS (*16*). Correction of $\chi$ for diamagnetism ($-19 \times 10^{-10}$ $m^3mol^{-1}$) and the Pauli susceptibility of the conduction electrons (positive but probably small because the $4d_{z^2}$ band is almost filled) will change the Curie constant somewhat. Correction for diamagnetism only leads to Curie constants which are about 3% larger. Curie constants larger than expected for $Ce^{3+}$ are in agreement with the presence of a small amount of $4f^2$ $Ce^{2+}$ with the $Ce^{2+}$ ($Pr^{3+}$) free ion Curie constant of $20.1 \times 10^{-6}$ $m^3Kmol^{-1}$ (*25*). Anisotropy in $\chi$, as observed for $(CeS)_{1.16}NbS_2$, is probably due to the crystal field splitting of the $^2F_{5/2}$ ground state of $Ce^{3+}$. The drop in $\chi^{-1}$ followed by a continuous decrease of $\chi^{-1}$ to zero is interpreted as a localization of presumably *5d* electrons, which leads to an increase in the number of $Ce^{2+}$ ions. For $(LaS)_{1.14}NbS_2$ (*18*) with 0.12 hole/Nb in the $4d_{z^2}$ band, the magnetic properties (Curie–Weiss behavior in the range 40–300 K) indicate 14% of La to be in the $La^{2+}$ $4f^1$ state, 86% of La is $La^{3+}$. For $(SmS)_{1.19}TaS_2$ (*6*) and $(GdS)_{1.21}NbS_2$ (*19*), the M–S distances of the rare earth sulfide part as well as the electrical and magnetic properties point to an almost filled $d_{z^2}$ band of $TS_2$ and trivalent rare earth metal in the *M*S part. SmS at normal pressure is a semiconductor with $Sm^{2+}$. Above 6 kbar it transforms into the collapsed state with $Sm^{3+}$ $(e^-)S^{2-}$. Unit cell dimensions of the HoS part in $(HoS)_{1.23}NbS_2$ (*26*) also point to trivalent Ho (solid HoS is also a metal with $Ho^{3+}$), but for $(YbS)_{1.14}NbS_2$ (*27*) the unit cell dimensions of the YbS part are in agreement with the lattice constant of solid YbS at normal pressure being a semiconductor with $Yb^{2+}$. At about 200 kbar YbS transforms to the collapsed state with $Yb^{3+}S^{2-}e^-$. Electrical transport properties and magnetic properties of the Ho and Yb compounds have not yet been measured. So far we have not been able to prepare a misfit layer compound with EuS in the *M*S part. Its structure and properties are of interest because Eu in EuS is also in the divalent state, like Yb in YbS.

## Acknowledgments

We thank Professor C. Haas and Dr. C. F. van Bruggen for valuable discussions on structure and physical properties.

## References

1. G. A. Wiegers, A. Meetsma, S. van Smaalen, R. J. Haange, P. J. Wulff, Th. Zeinstra, J. L. de Boer, S. Kuypers, G. van Tendeloo, J. van Landuyt, S. Amelinckx, A. Meerschaut, P. Rabu, and J. Rouxel, *Solid State Commun.* **70**(4) 409 (1989).
2. A. Meetsma, G. A. Wiegers, R. J. Haange, and J. L. de Boer, *Acta Crystallogr.* **A45**, 285 (1989).
3. G. A. Wiegers, S. van Smaalen, A. Meetsma, R. J. Haange, J. L. de Boer, A. Meerschaut, P. Rabu, and J.Rouxel, *Acta Crystallogr. B.*, **46**, 324 (1990).
4. J. L. de Boer, A. Meetsma, Th. J. Zeinstra, R. J. Haange, and G. A. Wiegers, *Acta Crystallogr. C.*, in press.
5. J. Wulff, A. Meetsma, S. van Smaalen, R. J. Haange, J. L. de Boer, and G. A. Wiegers, *J. Solid State Chem.* **84**, 118 (1990).
6. G. A. Wiegers, A. Meetsma, R. J. Haange, and J. L. de Boer, *J. Less-Common Met.*, in press.
7. A. Meerschaut, P. Rabu, and J. Rouxel, *J. Solid State Chem.* **78**, 35 (1989).
8. J. L. de Boer and A. J. Duisenberg, *Acta Crystallogr. A* **40**, C410 (1984).
9. A. L. Spek, Proceedings of the 8th European Crystallography Meeting, Liège, Belgium (1983).
10. L. E. McCandlish, G. H. Stout, and L. C. Andrews, *Acta Crystallogr. A* **24**, 321 (1968).
11. T. Hahn (Ed.), "International Tables for X-Ray

Crystallography," Vol A. Reidel, Dordrecht (1983).
12. D. T. CROMER AND J. B. MANN, *Acta Crystallogr. A* **24,** 321 (1968).
13. D. T. CROMER AND D. LIBERMAN, *J. Chem. Phys.* **53,** 1891 (1970).
14. HALL, S. R. AND STEWART, J. M., (Eds.) "XTAL2.2 User's Manual," Universities of Western Australia and Maryland (1987).
15. A. L. SPEK, *in* "Computational Crystallography" (D. Sayre, Ed), p. 528, Oxford University Press (Clarendon) London/New York (1982).
16. F. HULLIGER, B. NATTERER, AND H. R. OTT, *J. Magnet. Magn. Mater.* **8,** 87 (1978).
17. A. VAN DER LEE AND G. A. WIEGERS, *Acta Crystallogr. C,* **46,** 976 (1990).
18. G. A. WIEGERS AND R. J. HAANGE, *J. Phys.: Condens. Matter* **2,** 455 (1990).
19. G. A. WIEGERS, R. J. HAANGE AND J. L. DE BOER, to be published.
20. E. DONI AND R. GIRLANDA, "Electronic Structure and Electronic Transitions in Layered Materials" (V. Grasso, Ed.) Reidel, Dordrecht Holland (1986).
21. M. NAITI AND S. TANAKA, *J. Phys. Soc. Japan* **51,** 219 (1982).
22. W. G. FISHER AND M. J. SIENKO, *Inorg. Chem.* **19,** 39 (1980).
23. R. H. FRIEND AND A. D. YOFFE, *Adv. Physics* **36,** 1 (1987).
24. G. M. LOGINOV, A. T. STARAVOITOV, AND A. GOLUBKOV, *Sov. Phys. Solid State* **11,** 3053 (1970).
25. J. M. SMART, "Effective Field Theories of Magnetism", W. B. Saunders Co., Philadelphia and London (1986).
26. G. A. WIEGERS, R. J. HAANGE AND J. L. DE BOER, to be published.
27. A. MEERSCHAUT, P. RABU, J. ROUXEL AND G. A. WIEGERS, to be published.